Electronic Supplementary Material (ESI) for Nanoscale.

SUPPLEMENTRAY INFORMATION

Short Period Sinusoidal Thermal Modulation for Quantitative Identification of Gas Species

Aijun Yang†[a], Jifeng Chu†[a], Weijuan Li†[a], Dawei Wang[a], Xu Yang[a], Tiansong Lan[a], Xiaohua Wang*[a], Mingzhe Rong*[a] and Nikhil Koratkar*[bc]

---

[a] State Key Laboratory of Electrical Insulation and Power Equipment, Xi'an Jiaotong University, Xi'an 710049, PR China

[b] Department of Mechanical, Aerospace and Nuclear Engineering, Rensselaer Polytechnic Institute, Troy, NY 12180, USA

[c] Department of Materials Science and Engineering, Rensselaer Polytechnic Institute, Troy, NY 12180, USA

† These authors contributed equally

Supplementary Figures

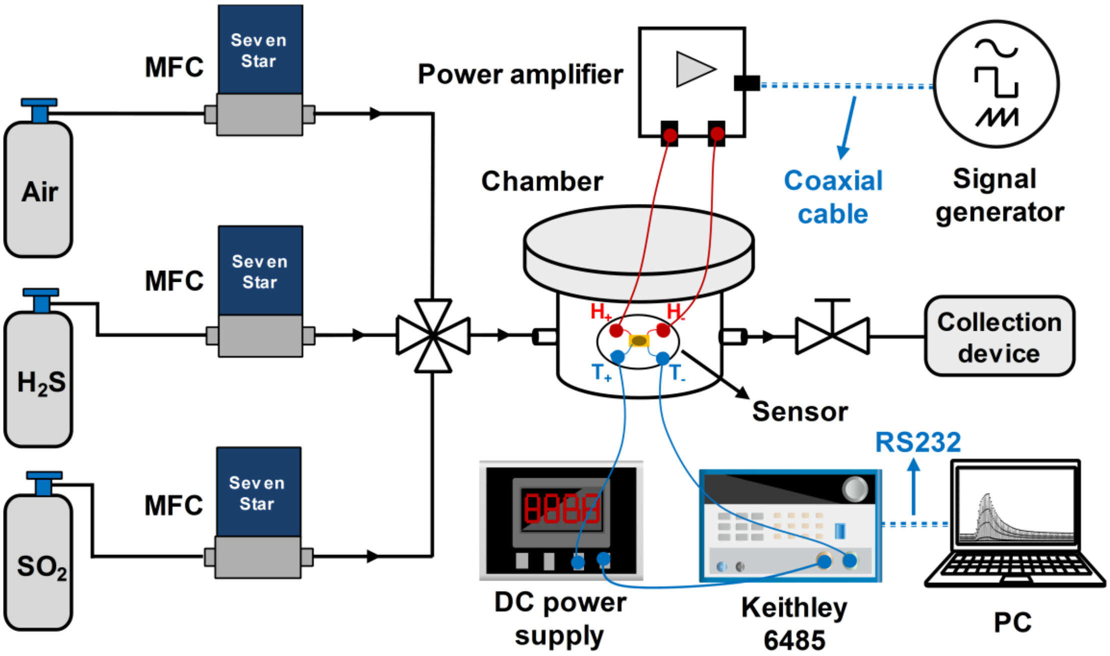

Fig. S1 Schematic illustration for gas sensing experimental device.

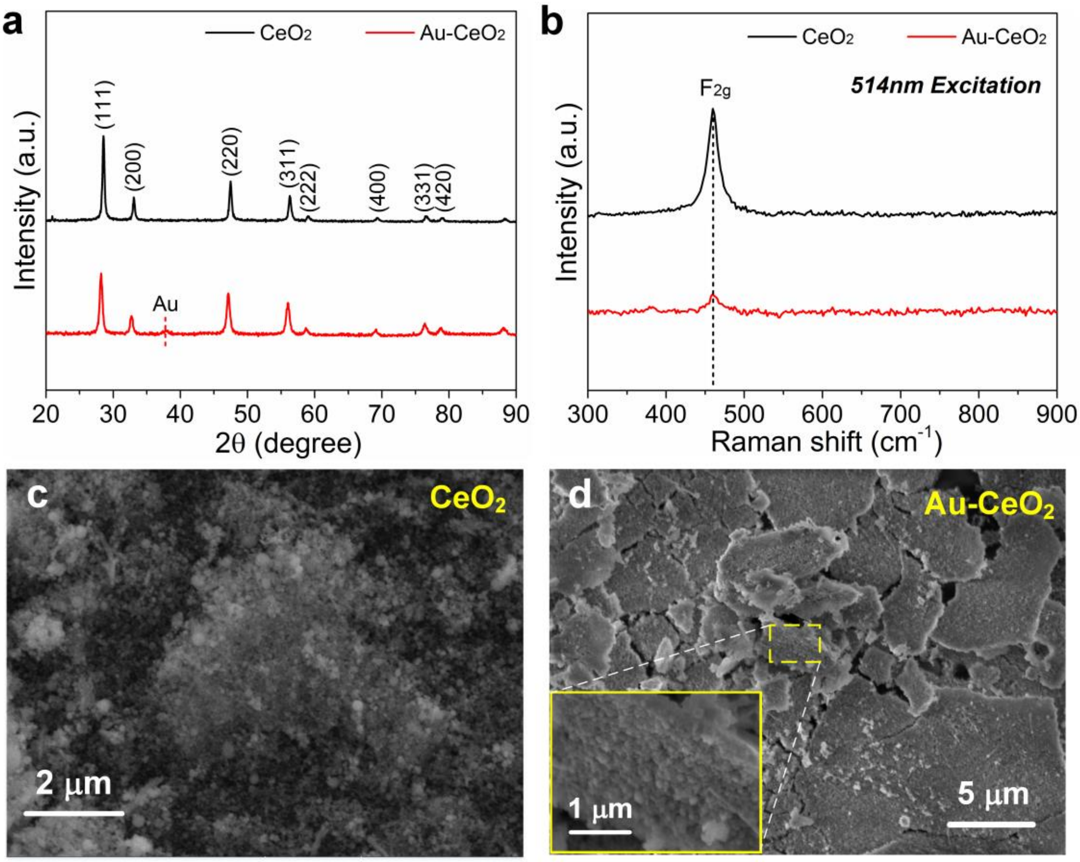

Fig. S2 (a) XRD spectra, (b) Raman spectra, and SEM images of (c) CeO_2 and (d) Au-CeO_2.

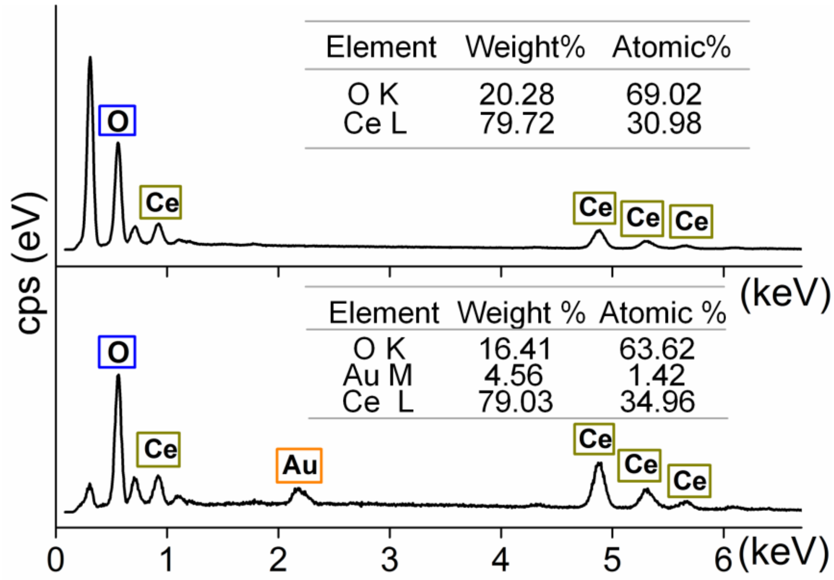

Element	Weight%	Atomic%
O K	20.28	69.02
Ce L	79.72	30.98

Element	Weight %	Atomic %
O K	16.41	63.62
Au M	4.56	1.42
Ce L	79.03	34.96

Fig. S3 EDS (point scan) of the pristine and functionalized CeO_2 samples.

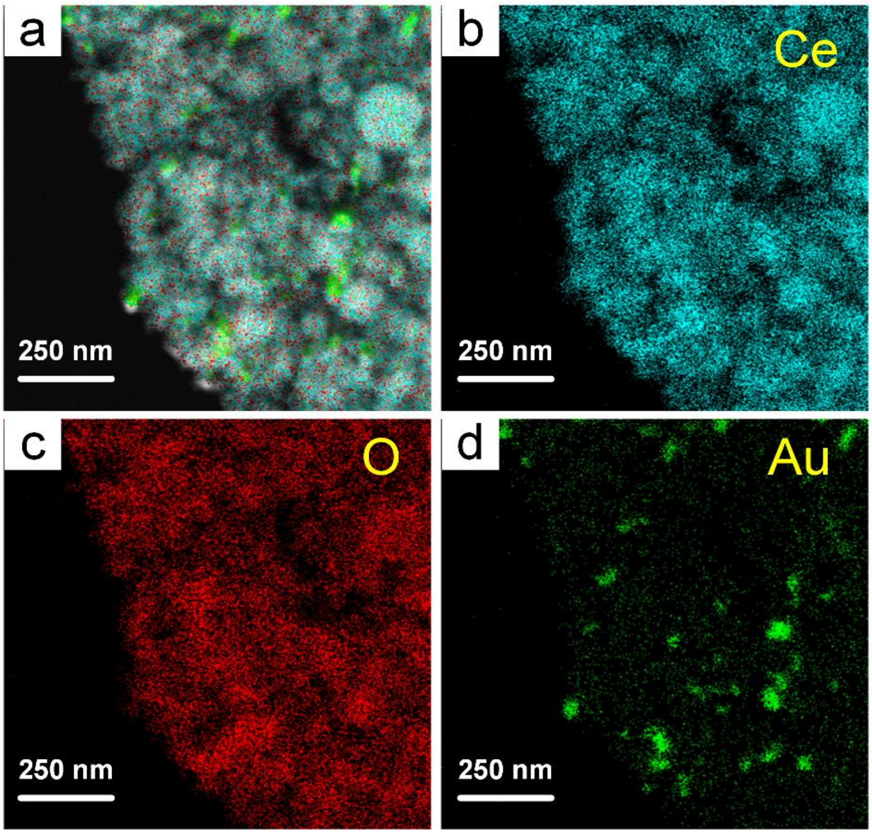

Fig. S4 (a) STEM Ce, O and Au mixed mapping image. (b) Ce, (c) O, (d) Au individual element mapping images of the as-prepared Au-CeO_2.

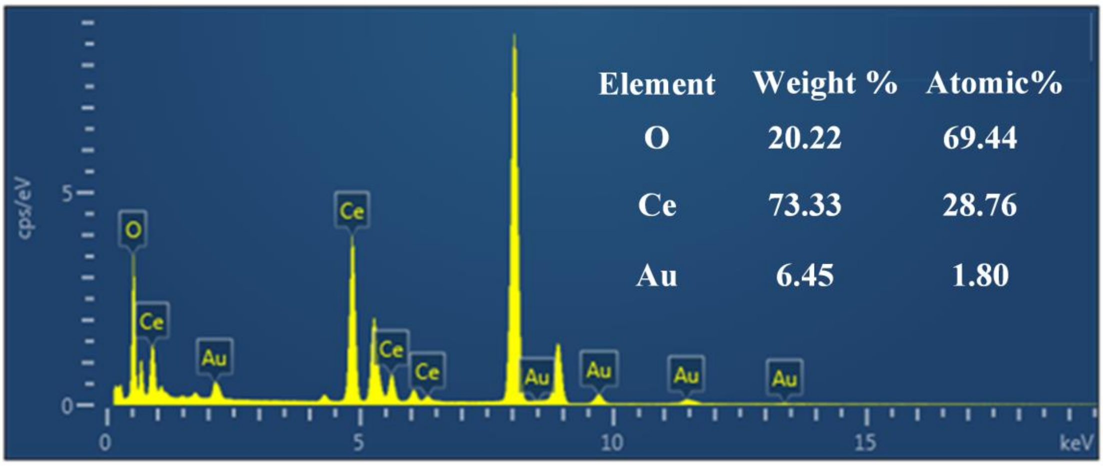

Element	Weight %	Atomic%
O	20.22	69.44
Ce	73.33	28.76
Au	6.45	1.80

Fig. S5 EDS (mapping scan) of Au-CeO_2 sample.

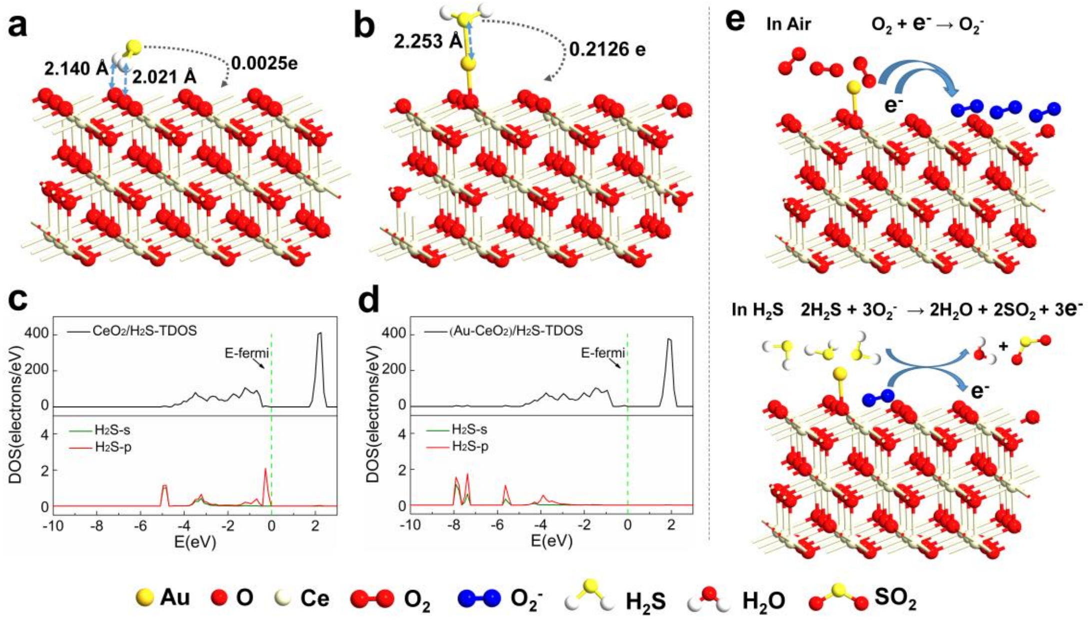

Fig. S6 The most stable adsorption structure of H_2S adsorbed on (a) pure ceria and (b) Au doped ceria. Density of states of H_2S adsorbed on (c) pure ceria and (d) Au doped ceria. (e) The probable mechanism of H_2S adsorption on the Au doped ceria surface in the presence of air. (Relevant atoms and molecules are represented at the bottom of the Figure.)

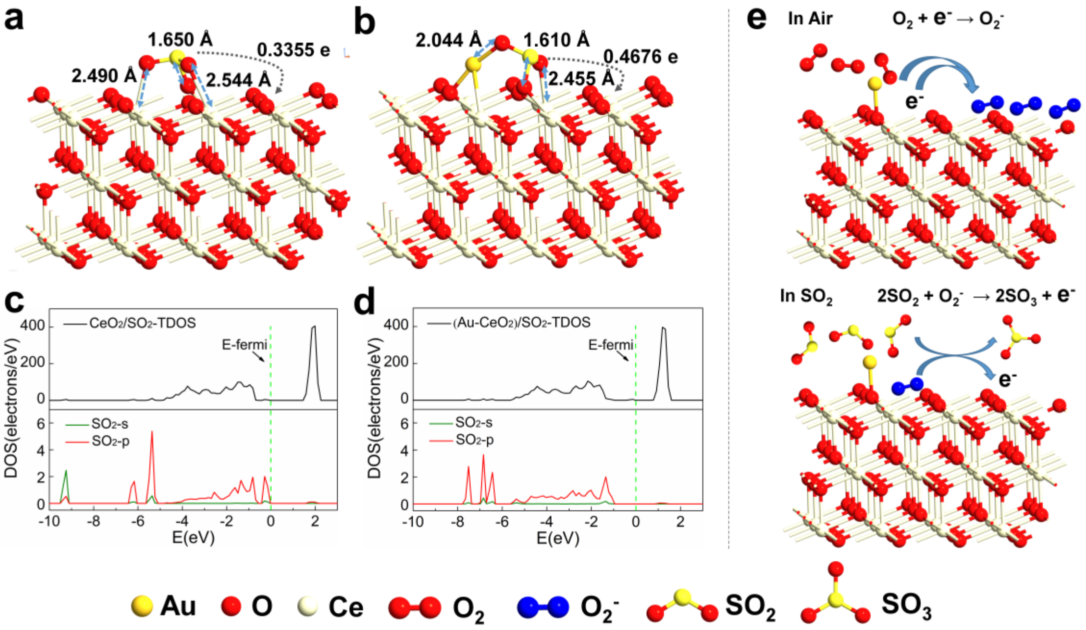

Fig. S7 The most stable adsorption structure of SO_2 adsorbed on (a) pure ceria and (b) Au doped ceria. Density of states of SO_2 adsorbed on (c) pure ceria and (d) Au doped ceria. (e) The probable mechanism of SO_2 adsorption on the Au doped ceria surface in the presence of air. (Relevant atoms and molecules are represented at the bottom of the Figure.)

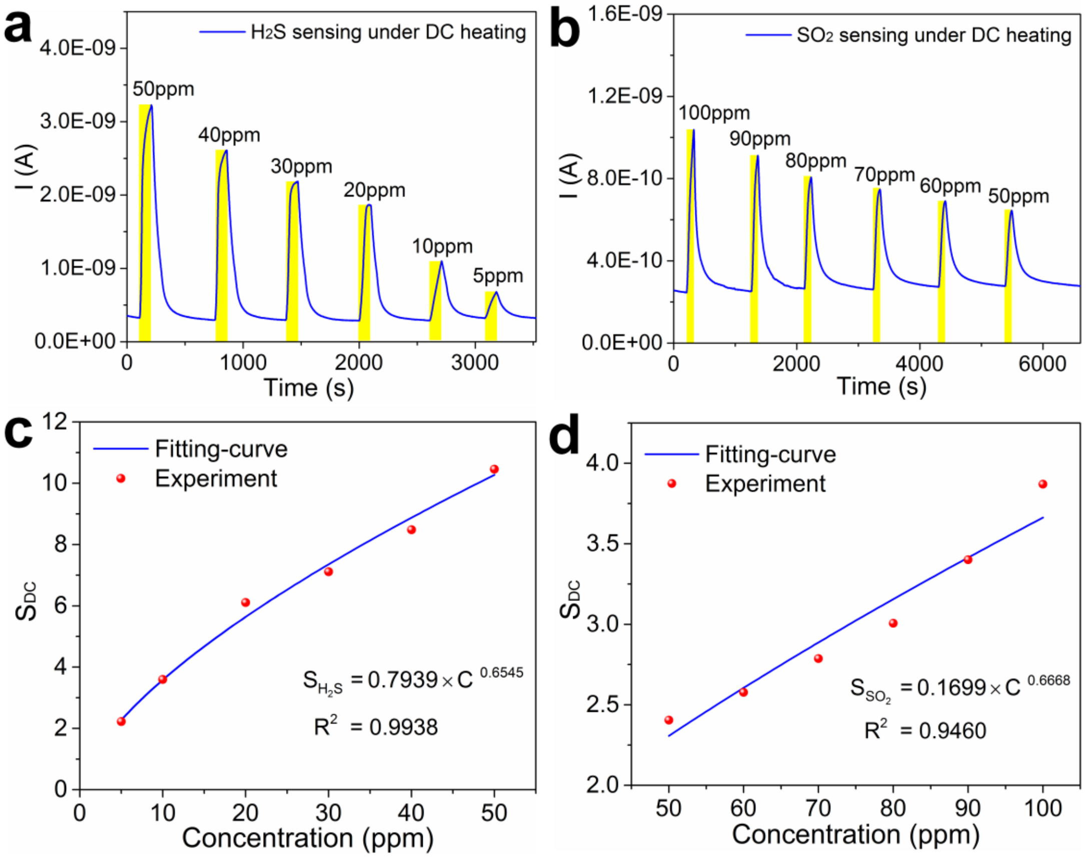

Fig. S8 Under DC heating voltage, the response-recovery curves of Au-CeO_2 sensor to various concentrations of (a) H_2S and (b) SO_2 at 100°C. Experimental results and fitting curves toward (c) H_2S and (d) SO_2, respectively.

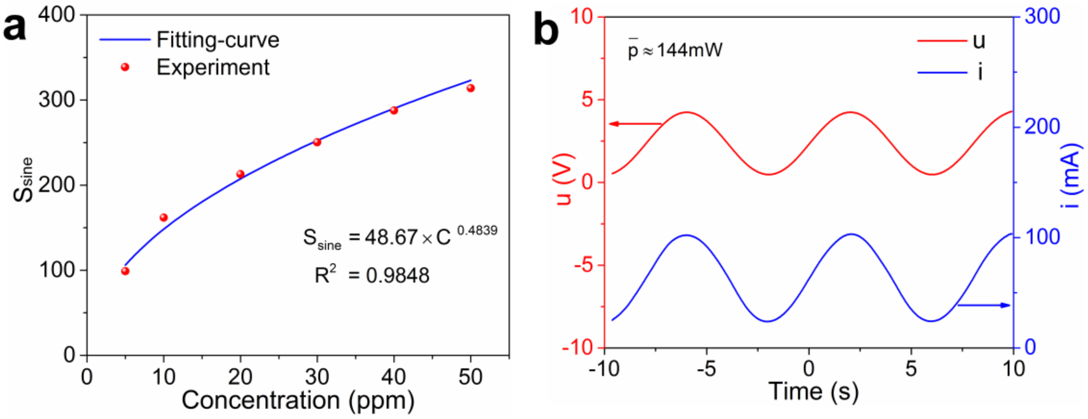

Fig. S9 (a) The responses of the sensor toward various concentrations of H_2S in the dynamic sensing experiment. (b) Current and voltage curves applied to the sensor's heating film.

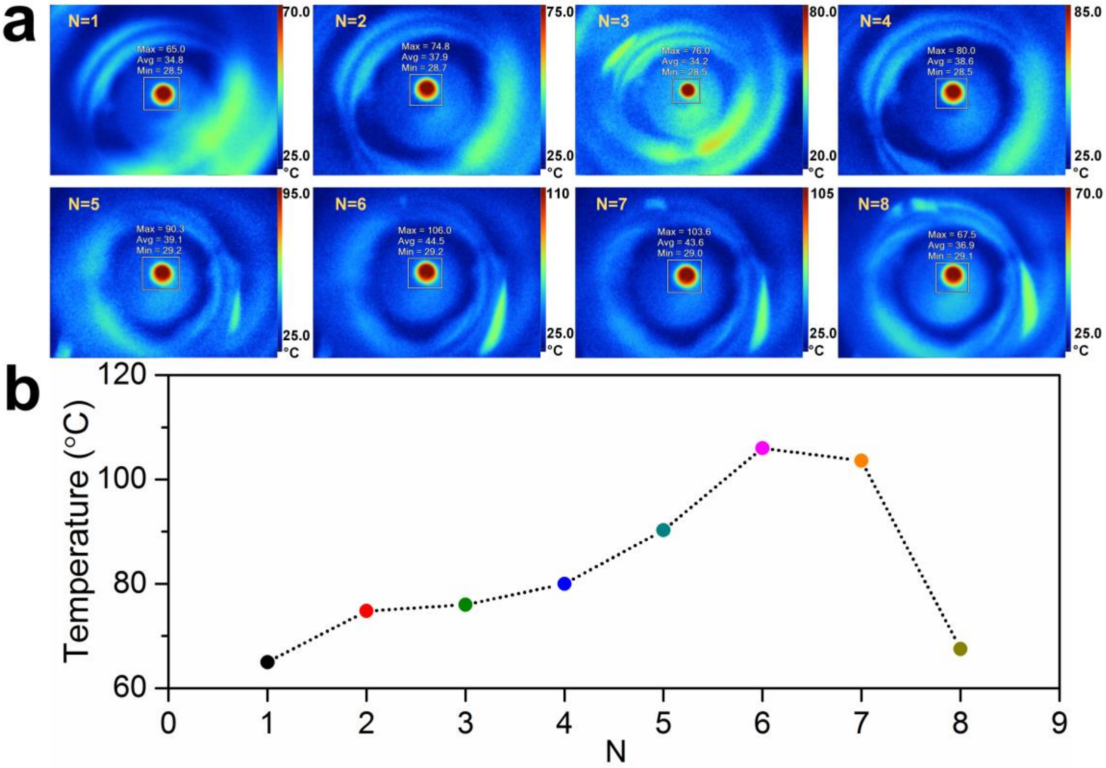

Fig. S10 During one sinusoidal heating cycle, (a) the corresponding temperature change monitored by the IR camera. (b) The maximum surface temperatures of the sensor at different sampling N.

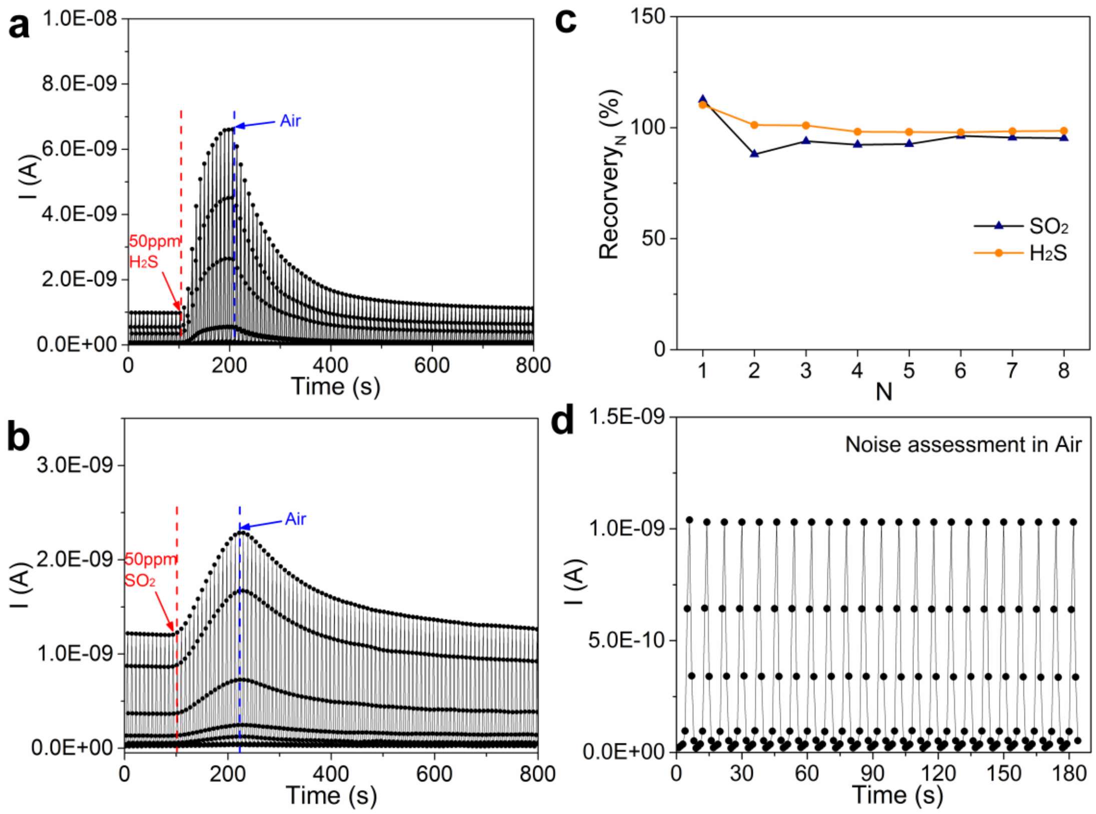

Fig. S11 The dynamic curves for sensing 50 ppm (a) H_2S and (b) SO_2. (c) Recovery capability of the sensor at different sampling N. (d) Noise assessment of the sensor current curve. The recovery capability of IN curve can be defined by: $\mathrm{Recovery_N} = \frac{I_{Ng} - I_{Na'}}{I_{Ng} - I_{Na}}$, where I_{Ng} represents the saturation sampling current value under the detected gas, I_{Na} represents the initial sampling current value under the background gas, and $I_{Na'}$ represents the final sampling current value under the background gas.

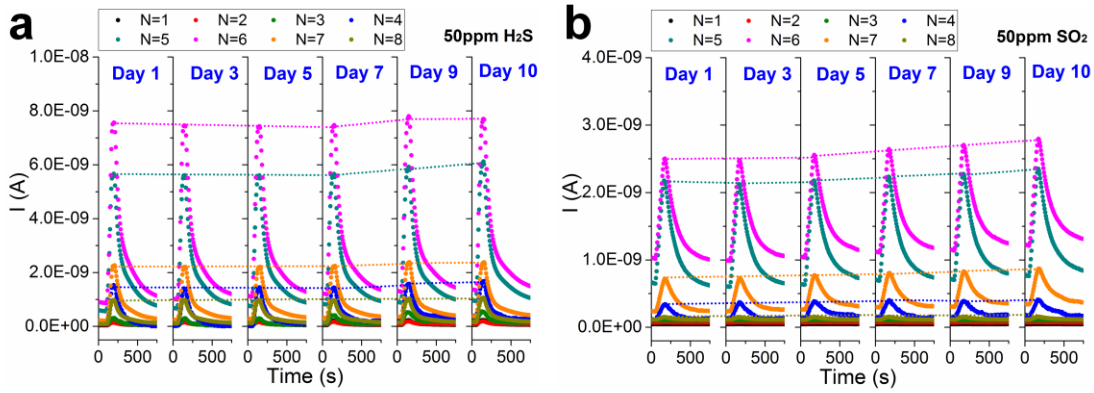

Fig. S12 The long-term stability of Au-CeO_2 sensor upon exposure to (a) 50 ppm H_2S and (b) 50 ppm SO_2.

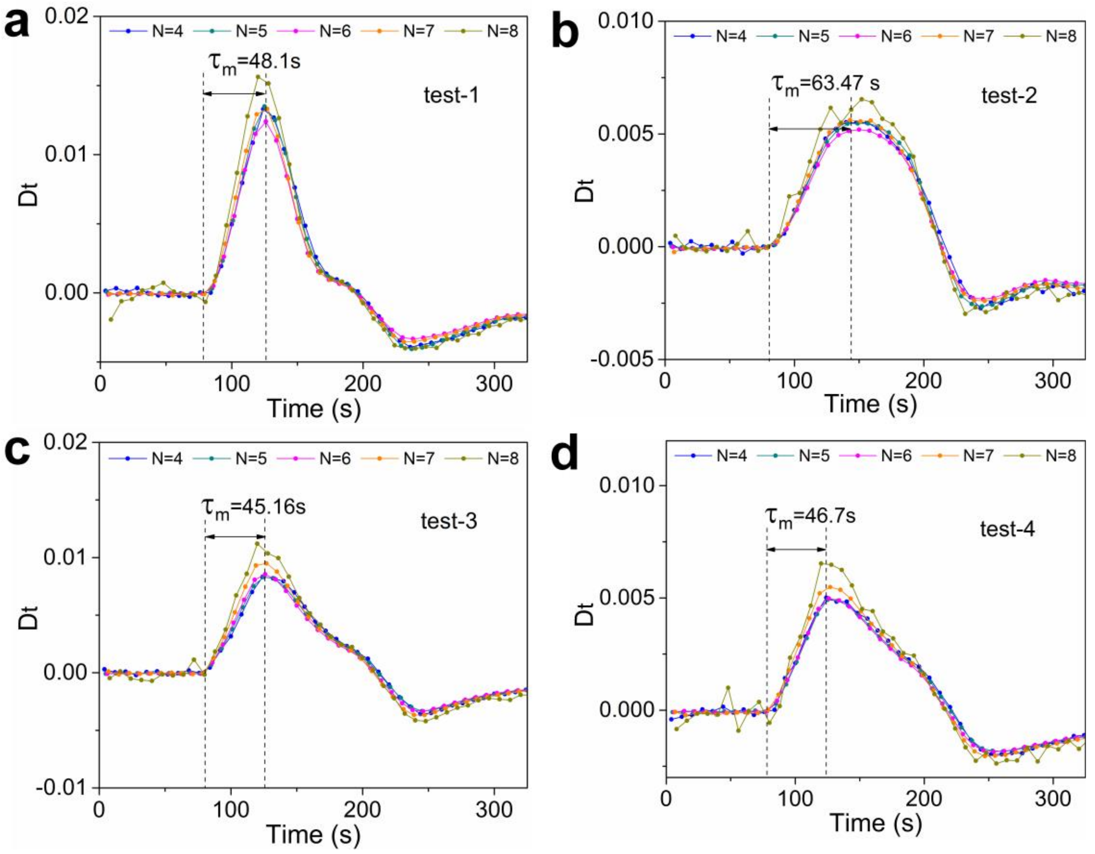

Fig. S13 Derivative curves at different sampling N for (a) test-1, (b) test-2, (c) test-3, (d) test-4.

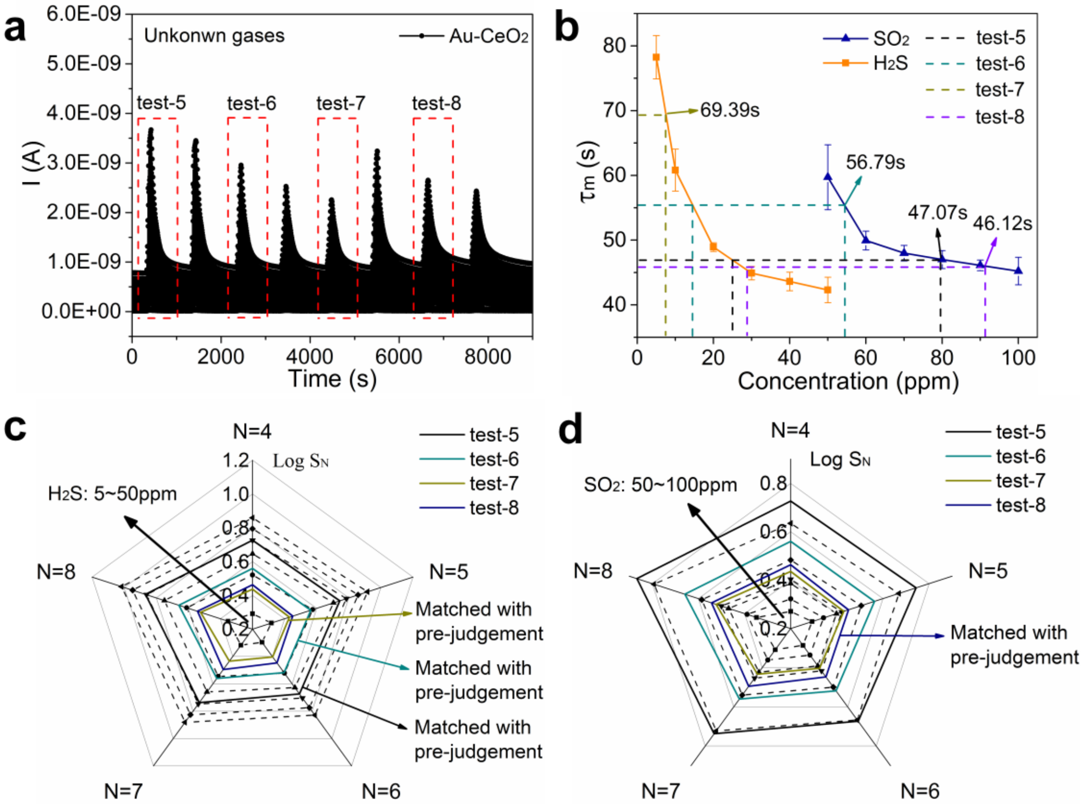

Fig. S14 (a) Variation of sensor current for different concentrations of H_2S and SO_2 (test gases) for four different test cases (i.e., test-5 through test-8). (b) The pre-judgements of the possible gases deduced by τ_m. The verifications of the pre-judgements by using radar charts of (c) H_2S and (d) SO_2.

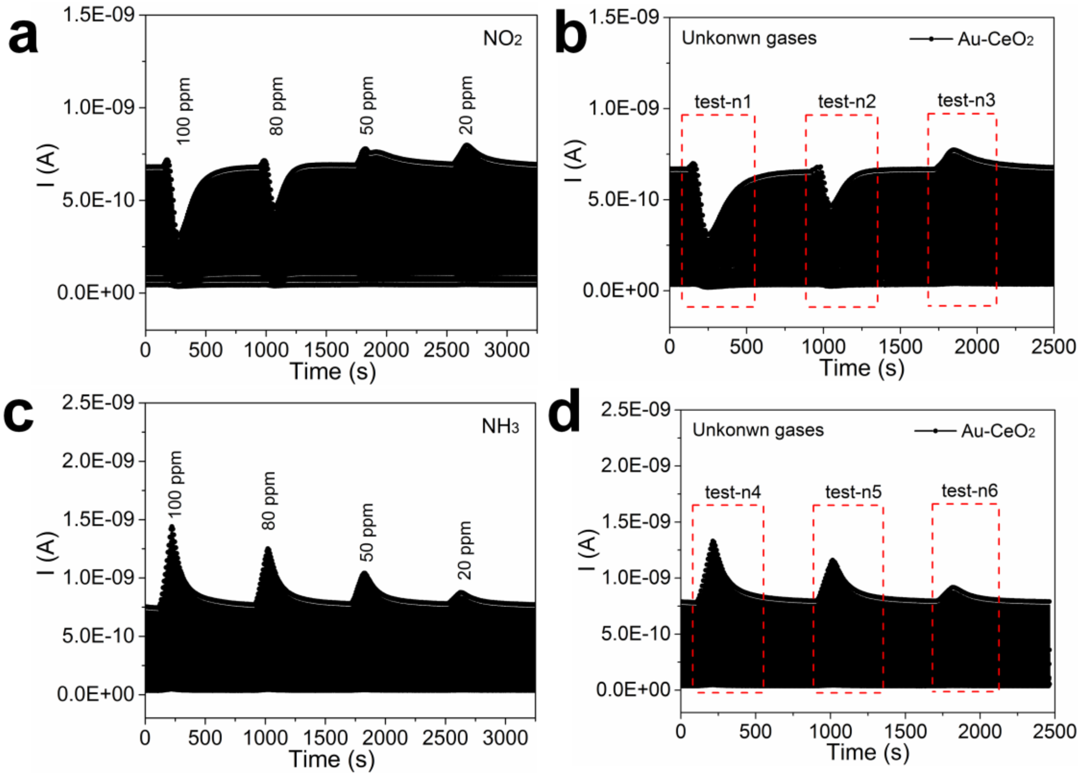

Fig. S15 The variation of sensor current for sensing (a) NO_2 and (c) NH_3 with various concentrations. (b), (d) The variation of sensor current toward unknown test gases (test-n1~n6) with different concentrations.

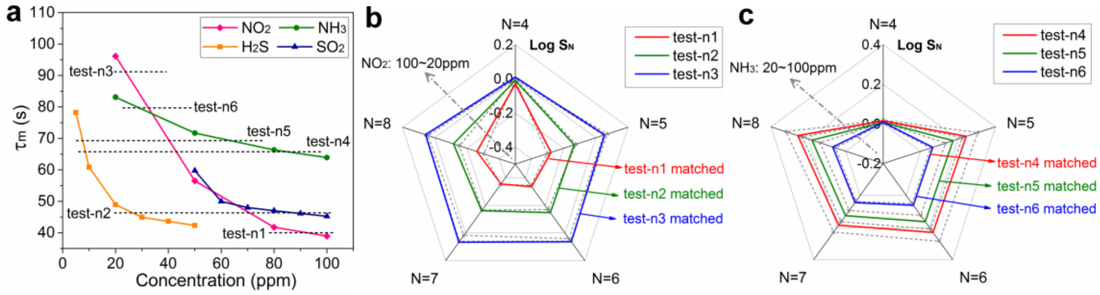

Fig. S16 (a) The pre-judgements of the possible gases deduced by τ_m. The verifications of the pre-judgements by using radar charts of (b) NO_2 and (c) NH_3.

Supplementary Tables

Table S1 The adsorption energy, the nearest distance, charge transfer and work function modification of H_2S adsorbed on both substrates

System	E_{ads}/eV	$d_{gas\text{-}ceria}$/Å	Q/e	ΔΦ/eV
H_2S/ceria	-0.424	(H_O)2.021	0.0025	-0.199
H_2S/Au-ceria	-2.175	(S_Au)2.253	0.2126	-0.564

Table S2 The adsorption energy, the nearest distance, charge transfer and work function modification of SO_2 adsorbed on both substrates

System	E_{ads}/eV	$d_{gas\text{-}ceria}$/Å	Q/e	ΔΦ/eV
SO_2/ceria	-1.216	(O_Ce)2.490	0.3355	-0.371
SO_2/Au-ceria	-2.783	(S_O)1.610	0.4676	0.194

Table S3 The relationship between τ_N and the H_2S concentration at different sampling N

τ_N (s)	Concentration					
	5 ppm	10 ppm	20 ppm	30 ppm	40 ppm	50 ppm
τ_4	75.32	62.126	48.554	46.152	44.868	43.44
τ_5	76.5	63.407	49.12	45.521	44.618	44.598
τ_6	77.262	63.703	49.698	45.11	44.076	42.78
τ_7	78.218	58.577	47.994	43.656	43.243	41.179
τ_8	83.913	56.311	49.323	44.1	41.326	39.575
τ_m	78.2426	60.8248	48.9378	44.9078	43.6262	42.3144

Table S4 The relationship between τ_N and the SO_2 concentration at different sampling N

τ_N (s)	Concentration					
	50 ppm	60 ppm	70 ppm	80 ppm	90 ppm	100 ppm
τ_4	67.52	48.291	46.856	46.063	45.86	48.716
τ_5	61.494	47.643	47.5	46.4102	46.19	44.826
τ_6	58.577	50.731	49.11	48.343	47.45	45.085
τ_7	55.474	47.76	47.065	48.641	45.86	44.604
τ_8	55.569	50.291	49.45	45.62	45.233	42.9
τ_m	59.7268	48.9432	47.9962	47.01544	46.1186	45.2262

Table S5 Summary of identification results (test n1~n6).

Test	Pre-judgement	Identification	True value	Error (%)
n1	93ppm NO_2	93ppm NO_2	90ppm NO_2	3.33
n2	72ppm NO_2	72ppm NO_2	70ppm NO_2	2.86
	26ppm H_2S			
	87ppm SO_2			
n3	23ppm NO_2	23ppm NO_2	20ppm NO_2	15.00
n4	43ppm NO_2	83ppm NH_3	85ppm NH_3	2.35
	83ppm NH_3			
	8ppm H_2S			
n5	40ppm NO_2	68ppm NH_3	65ppm NH_3	4.62
	68ppm NH_3			
	7ppm H_2S			
n6	32ppm NO_2	28ppm NH_3	25ppm NH_3	12.00
	28ppm NH_3			

Supplementary Texts

Under the action of sinusoidal heating voltage, the response value of the sensor is defined as follows:

$$S_{sine} = I_{Ng\_max}/I_{Na\_min} \tag{S1}$$

where I_{Na_min} is the minimum value of I_N curves in the background gas, and I_{Ng_max} is the maximum value of I_N curves in the detected gas.

For evaluating the detection limits (DL) of the sensor toward H_2S, the noise formula is given as follows:

$$S_{DL} = (1 + 3 * \text{Noise}_6) * \frac{M_6}{M_1} \tag{S2}$$

where M_6 is the mean of the I_N curve at sampling sixth in air, and M_1 is the mean of the I_N curve at sampling first in air. Noise_6 is calculated to 0.202% as shown in Table 1 of main manuscript.

The adsoption energy (E_{ads}), basically used to characterize the adsorption intensity, is defined as [1]:

$$E_{ads} = E_{molecule/substrate} - E_{molecule} - E_{substrate} \tag{S3}$$

where $E_{molecule/substrate}$, $E_{molecule}$ and $E_{substrate}$ represent the energies of the substrate with the gas molecule, isolated gas molecule, and the substrate, respectively. By this definition, a negative adsorption energy mean that the adsorption was exothermic, and higher negative values correspond to stronger adsorptions.

The modification of work function energy of the substrate with and without the gas molecule adsorbed was also an important indicator of adsorption. The definition of work function energy is [2]:

$$\Phi = E_{vacuum} - E_{Fermi} \tag{S4}$$

in which, E_{vacuum} and E_{Fermi} refer to vacuum energy and Fermi energy respectively.

Fig. S7a and E_{ads} of SO_2 adsorbed on ceria (111) listed in Table S2 show that SO_2 is chemically adsorbed on pure ceria surface, with 0.3355 electrons transferring to the substrate. While, the interaction between SO_2 and Au-ceria (111) was stronger for the larger adsorption energy and charge transfer value (**Fig. S7**b). Besides, the peak of the 2p orbital near Fermi level of SO_2 in plot of DOS (**Fig. S7**c) indicates a tight interaction occurring between SO_2 and ceria (111) surface. Similar to the adsorption of H_2S, the Fermi level of TDOS in **Fig. S7**d is upshifted compared with that in Fig. S4c, which indicates greater electron transfer from gas molecules to substrate when SO_2 molecules interacted with the Au-ceria (111) surface. **Fig. S7**e is a possible adsorption mechanism of SO_2 on the Au-ceria (111) surface in the presence of air (oxygen).

To prove the broad application of this two-steps judgement process, we have supplemented experiments for quantitatively detecting NO_2 and NH_3 with concentrations ranging from 20ppm to 100ppm, respectively. Experimental conditions are consistent with those described in the manuscript. Firstly, the recognition library is established based on the known gas concentrations (100ppm, 80ppm, 50ppm, 20ppm). **Fig. S15**a and **S15**c presents the variation of sensor current for sensing NO_2 and NH_3 with various concentrations.

Similarly, the τ_m values of Au-CeO_2 sensor for NO_2 and NH_3 detection are respectively given in **Fig. S16**a, it's obvious that there are obvious differences between these two curves. Extracting S_N by sampling from the sampling fourth (N=4) to the sampling eighth (N=8), we can develop an envelope by sequentially connecting every S_N at a fixed gas concentration, and then a radar chart is constituted by a series of envelopes at various concentrations, as shown in **Fig. S16**b and **S16**c. With this, the dependence of τ_m on gas concentration and the radar chart, together constitute the gas recognition library, which could be used to quantitatively identify NO_2 and NH_3.

To evaluate the accuracy of recognition library, we have also measured a series of sensor current curves when exposed to test gases (test n1~n6), as presented in Fig. S15b and S15d. Then, we use the library to discriminate the concentration of unknown gas via a two-step judgment. Take test-n2 and test-n5 as examples, the reliability of library is evaluated. For test-n2, τ_m is 45.36s and it is evident that the test gas is ~72 ppm NO_2, ~26ppm H_2S or ~87ppm SO_2. As shown in **Fig. S16**b, the green envelope for test-n2 is between 50ppm and 80 ppm NO_2, and it's very closed to 80ppm. Conversely, it doesn't match with the H_2S envelopes in Fig. 4c or the SO_2 envelopes in Fig. 4d. Therefore, test-n2 can be identified as ~72ppm NO_2. While for test-n5, τ_m is 68.72s and therefore the test gas could be ascribed to ~40ppm NO_2, ~68ppm NH_3, or ~7ppm H_2S. Then, NO_2, NH_3 and H_2S radar charts are analyzed to verify the pre-judgements of test-n5. In **Fig. S16**c, we can find that the green envelope is located between 50ppm and 80ppm NH_3, yet it can't be matched with the NO_2 envelopes in **Fig. S16**b or the H_2S envelopes in Fig. 4c. So, test-n5 is detected as ~68ppm NH_3, which is relatively consistent with the actual concentration (65ppm NH_3).

We have summarized the identification results of test-n1 through test-n6 in **Table S5**. It is evident that the gas recognition library can be used to discriminate NO_2 and NH_3 in a facile manner and the maximum recognition error is less than 15%. Therefore, the supplemented experiments have verified that the short period sinusoidal thermal modulation strategy has ability to be broad application for quantitatively detecting sorts of gases.

Supplementary References

1 J. Zhang, X. Q. Gong and G. Z. Lu, *Chinese J. Catal.*, 2014, **35**, 1305-1317.

2 D. W. Wang, X. H. Wang, A. J. Yang and P. Lv, *Mater. Chem. Phys.*, 2018, **212**, 453-460.